


Interacting Electrons in Two-Dimensional Electride Ca_2N

Dmitry Y. Novoselov,* Dmitry M. Korotin, Alexey O. Shorikov, Vladimir I. Anisimov, and Artem R. Oganov

 Cite This: *J. Phys. Chem. C* 2021, 125, 15724–15729

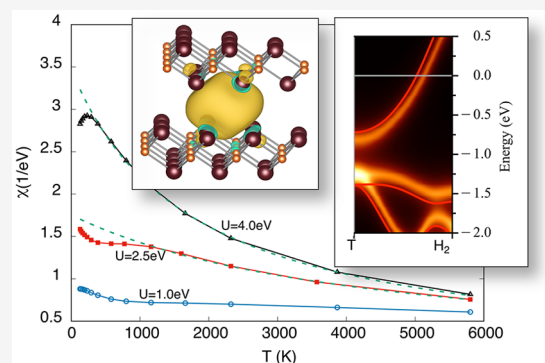
 Read Online

ACCESS |

 Metrics & More

 Article Recommendations

ABSTRACT: We investigated the role of correlation effects in the formation of the spectral and magnetic properties of two-dimensional electride Ca_2N . Using the combination of Density Functional Theory with Dynamical Mean-Field Theory (DFT+DMFT), we found that Coulomb interactions between the electrons of the electride states cause a strong renormalization and shift of the energy bands near the Fermi level. Besides, the electronic correlations lead to a competition between the Stoner-type ferromagnetic instability and the antiferromagnetic interactions of the localized moments. The observed patterns should be inherent to other isostructural electrides.



INTRODUCTION

The term “electrides” coined by James Dye¹ describes a rather broad class of materials that have electrons confined in the interstices of the crystal structure. The topology and dimensions of these cavities determine primarily the properties of anionic electrons, including the mobility and degree of localization, especially if the energy bands of these excess electrons cross the Fermi level. These electrons can participate in complex interactions with each other and with cations. As a result, electrides exhibit diverse properties, providing a rich field for experiments and a challenge for theoretical research. A high density of anionic electrons and low binding energy make such materials very promising for a variety of practical applications, particularly as efficient electron emitters² and high-performance catalysts.^{3–6}

When a new class of low-dimensional electronic systems with a layered structure was discovered, the first among them, dicalcium nitride,⁷ immediately attracted the attention of researchers.^{8–20} Recently, the existence of several two-dimensional electrides isostructural to Ca_2N has been confirmed,^{21–23} including Sr_2N , Ba_2N , Sc_2C , Gd_2C , Tb_2C , Dy_2C , Ho_2C , and Y_2C . Dicalcium nitride is a two-dimensional electride (Q2DE) with the chemical formula $[\text{Ca}_2\text{N}]^+ \cdot e^-$ and has an anti- CdCl_2 crystal structure with an $R\bar{3}m$ space group. The anionic electrons in this system are confined in the interlayer voids between the Ca layers.

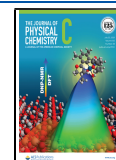
It was shown that Ca_2N undergoes a metal-to-semiconductor transition under pressure²⁴ closely associated with a change in the degree of localization of anionic electrons responsible for the transport properties of an electride. An intrinsic negative in-plane dispersion of the anionic plasmon

(collective oscillations of the density of the free electron gas), revealed using the first-principles time-dependent density functional theory calculations,¹² is in striking contrast with what could be expected for a homogeneous electron gas. The temperature dependence of the resistivity of Ca_2N is quadratic, which indicates the presence of Coulomb interactions between the electrons responsible for the transport properties.⁷ The measurements of the anisotropic magnetoresistance make it possible to argue that the electron–electron interaction in Ca_2N is stronger than in metallic Ca because the electrons do not propagate over the entire crystal but are localized in a much tighter space.^{7,25,26} The experimental data⁷ demonstrate a large enhancement of the effective electron mass, 1.9–2.5 m_0 , in Ca_2N . The band structure calculations for this system show that a single band with a width of 2.5 eV which crosses the Fermi level E_F consists mainly of nonatomic electronic states centered between the $[\text{Ca}_2\text{N}]^+$ layers with small contributions from the atomic orbitals of Ca and N. This indicates that the electrical conductivity of Ca_2N is due to the electrons enclosed in the space between the layers. The experimental work²⁷ has shown that the results of DFT calculations do not correctly describe the positions of the energy bands that do not coincide well with the angle-resolved photoemission spectroscopy

Received: May 21, 2021

Revised: June 20, 2021

Published: July 9, 2021



(ARPES) results.⁷ Thus, the available data indicate that Ca₂N can behave as a strongly correlated material and it is important to understand how the Coulomb correlations affect the physical properties of Ca₂N, as well as other isostructural electrides. Unfortunately, there is no direct experimental evidence of the presence of magnetic moments in Ca₂N. Since correlations are expected on electride states which are localized between atomic layers, and their wave functions are a combination (superposition) of atomic ones, the magnetic properties and behavior of electrons should be different from what we expect for well-localized d- or f-electrons. In its turn, it makes it difficult to apply standard experimental methods to estimate the magnitude of local magnetic moments.

In the present paper we evaluate the strength of the Coulomb interactions of anionic electrons and investigate the influence of correlation effects on the spectral and magnetic properties of the two-dimensional electride Ca₂N.

METHODS

In the present study we used the combination of DFT and DMFT methods which provides the most unambiguous way to investigate the electronic structure. The DFT calculations were carried out with VASP²⁸ and Quantum ESPRESSO packages,²⁹ using the PBE exchange-correlation functional.³⁰ The results of the latter were used to construct the Hamiltonian in the Wannier function (WF) basis using the Wannier90 package³¹ for extraction the noninteracting GGA Hamiltonian H_{GGA} in the real space and transformation to the reciprocal space. The VASP package was used for the estimation of the Coulomb U parameter using a localized basis of atomic orbitals by the linear response approach.³² Coulomb correlations were taken into account for the constructed Hamiltonian within the DFT+DMFT approach.

This method allows taking into account many-body effects such as Coulomb correlations within the dynamical mean-field theory (DMFT).^{33,34} On the first step an effective Hamiltonian H_{DFT} was constructed on the basis of the Wannier functions using realistic noninteracting band structure $\varepsilon(\vec{k})$ obtained within the DFT for the compound under consideration. Finally, full many-body Hamiltonian which is solved within the DFT+DMFT has the form:

$$\hat{H} = \hat{H}_{\text{DFT}} - \hat{H}_{\text{DC}} + \frac{1}{2} \sum_{i,m,m',\sigma,\sigma'} U_{m,m'}^{\sigma,\sigma'} \hat{n}_{i,m,\sigma} \hat{n}_{i,m',\sigma'} \quad (1)$$

Here $U_{m,m'}^{\sigma,\sigma'}$ is the Coulomb interaction matrix and $\hat{n}_{i,m,\sigma}$ is the occupation number operator for the correlated electride electrons with orbital and spin indices i,m,σ at the i th site. The elements of $U_{m,m'}^{\sigma,\sigma'}$ matrix were parametrized by the on-site Hubbard parameter U and Hund's intra-atomic exchange J_{H} according to the procedure described in ref 35. Since the electride state is nondegenerate and has only two spin-orbitals J_{H} was set to 0 eV in the present calculations for the sake of simplicity.

The DFT+DMFT calculations were performed for the inverse temperature values β from 2 to 90 eV⁻¹, where $\beta = 1/k_{\text{B}}T$, k_{B} is the Boltzmann constant, and T is the absolute temperature. We used the simplified fully localized limit form for double-counting correction: $\hat{H}_{\text{DC}} = \bar{U}(N - 1/2)\hat{I}$ in a self-consistent DMFT loop, where N is the total self-consistent number of electrons on the electride site obtained within the DFT+DMFT, \bar{U} is the average Coulomb parameter for the electride shell, and \hat{I} is the identity operator. The continuous-

time quantum Monte Carlo hybridization expansion solver from the AMULET package³⁶ was applied to solve the effective DMFT quantum impurity problem.³⁷ The analytical continuation of the self-energy dependence on the real frequencies was obtained by using the Padé approximation method.³⁸

RESULTS AND DISCUSSION

To describe the electronic states localized between the atomic layers, we used the maximally localized Wannier functions (MLWFs).³¹ Four MLWFs were constructed within the energy window spanned by one energy band crossing the Fermi level and three lower-energy bands (Figure 1a). The first obtained

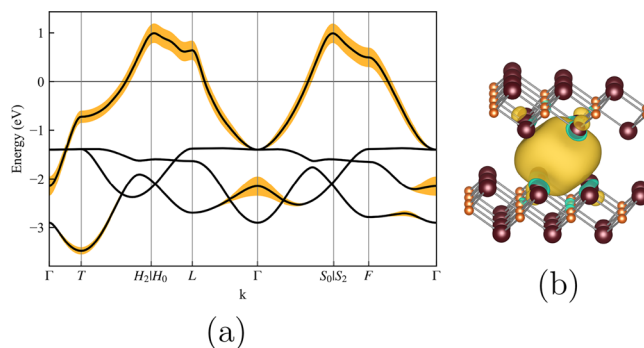


Figure 1. (a) Band structure of Ca₂N (black lines). The contribution to the Bloch states by the maximally localized Wannier function with s-symmetry centered on the electride layers is shown in yellow. High-symmetry points in the Brillouin zone correspond to the rhombohedral unit cell. (b) Spatial distribution of the MLWF describing the electride state. The Ca and N atoms are shown in reddish-purple and orange, respectively.

MLWF is centered in the crystal void at position (0.5, 0.5, 0.5), has the symmetry of an s-orbital (Figure 1b), and represents the electride state.^{10,39} The contribution of the first MLWF to the band structure is shown in Figure 1a. The other three MLWFs have a symmetry of p-orbitals, are centered on the nitrogen atoms, and describe three fully occupied energy bands in the interval [-3.5; -1.2] eV. The noninteracting Hamiltonian constructed in the basis of the obtained Wannier functions was solved in the framework of the DMFT method.^{33,34,36} The dependences of the self-energy on the Matsubara frequencies and Green's functions on the imaginary time τ , obtained in DMFT calculations, are presented in Figure 2. The value of the Green's function at the point $\beta/2$ on the imaginary time domain indicates the metallic character of conductivity at intermediate values of U and a tendency to transition to the semimetallic state at $U = 4$ eV caused by the splitting of the half-filled double degenerate electride band into a completely filled and an empty one. The self-energy function for $U = 4$ eV tends to diverge at zero, indicating a sharp increase in the localization of the electronic states at the electride site (Figure 2).

The analytical continuation of the self-energy dependence on the real frequencies and evaluated the spectral functions is shown in Figure 3. For a small value of $U = 1$ eV, the spectral function of the electride states resembles the DOS obtained using DFT. An increase of U up to 2.5 eV leads to a renormalization of the spectral weight and narrowing of the band around the Fermi level. Well-pronounced upper and lower Hubbard bands appear at +1.8 eV and -1.0 eV, respectively. A further increase of the Coulomb interaction

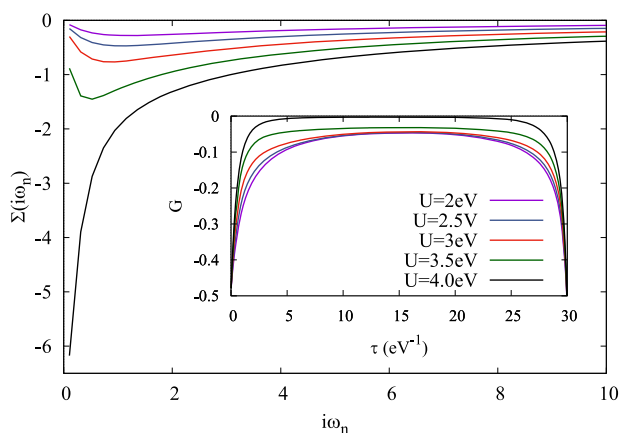


Figure 2. Imaginary part of the self-energy as a function of Matsubara frequencies at $\beta = 30 \text{ eV}^{-1}$ for different values of Coulomb parameter U and corresponding Green's functions in the inset.

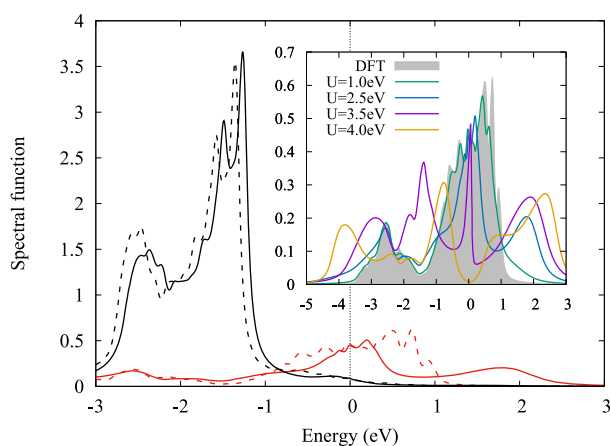


Figure 3. Spectral functions obtained using DFT (dashed lines) and DFT+DMFT (solid lines) for $\beta = 30 \text{ eV}^{-1}$ and $U = 2.5 \text{ eV}$ resolved for the electride (red) and p -N (black) states. The spectral functions of the electride states obtained using DFT and DMFT for different values of U are shown in the inset. Zero corresponds to the Fermi energy.

parameter up to 3.5 eV enhances the formation of the quasiparticle peak at the Fermi level and the upper and lower Hubbard bands. For $U = 4 \text{ eV}$, the transition to the semimetallic state close to that of a Mott insulator is accomplished. The behavior of the spectral function obtained using DMFT for Ca_2N resembles the results of the one-band Hubbard model with half-filling. The bandwidth of the electride state is $\approx 2.0\text{--}2.2 \text{ eV}$. The value of the Coulomb interaction was varied from 2 to 4 eV, which yielded the ratio between the Coulomb parameter and the bandwidth U/W from 1 to ≈ 2 . The former corresponds to the intermediate correlated metallic regime, and the latter corresponds to the insulating state. The dynamic Coulomb correlations lead to a strong renormalization of the band structure and a shift of the Fermi level. The magnitude of the shift depends on the Coulomb interaction parameter U and the electronic temperature $T = 1/k_B\beta$. We calculated the effective electron mass enhancement $m^*/m = 1 - \frac{\partial \Sigma}{\partial \omega}|_{\omega=0}$ for the U values from 2 to 3.5 eV (Table 1). We have estimated the upper bound of the U parameter using a more localized basis of atomic orbitals by the linear response approach³² as implemented in VASP and

Table 1. Effective Electron Mass Enhancement m^*/m and the Fermi Level Shift Relative to DFT Value Obtained Using DMFT at $\beta = 30 \text{ eV}^{-1}$. The Experimentally Determined Electron Mass Enhancement is 1.9–2.5.⁷

U (eV)	2	2.5	3	3.5
m^*/m	1.74	2.35	3.62	9.21
ΔE_F (eV)	0.07	0.09	0.12	0.16

obtained the value of about $\approx 2.78 \text{ eV}$. The resulting effective U on MLWFs should have a slightly smaller value due to more effective screening. At $U = 2.5 \text{ eV}$, the m^*/m equals $2.35m_0$, which agrees better with the experimental value of 1.9–2.5 m_e ⁷ and the paramagnetic solution with a local instant squared magnetic moment of $0.76 \mu_B$ per electride site.

To analyze the effect of dynamic correlations on the Ca_2N band structure and compare it with the experimental ARPES data,²⁷ we evaluated the energy dispersion along H-A-H and K- Γ -K directions of the Brillouin zone (Figure 4). A comparison

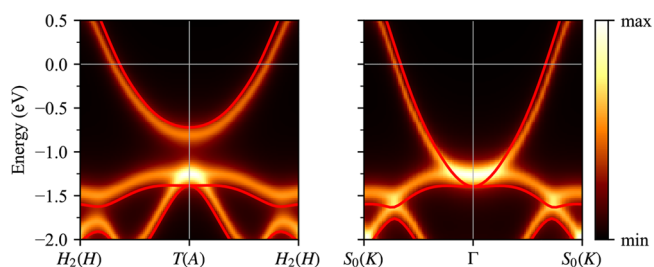


Figure 4. ARPES in H_2 -A- H_2 (corresponds to H-A-H in the hexagonal unit cell) and S_0 - Γ - S_0 (K- Γ -K in the hexagonal unit cell) directions obtained in DMFT calculations at $\beta = 60 \text{ eV}^{-1}$ with $U = 2.5 \text{ eV}$. Band structure from the DFT calculations is shown by the solid red lines.

of DFT bands and the ARPES data obtained using DMFT leads to a conclusion that accounting for the dynamic Coulomb correlations between the confined electrons results in smearing and shift of the electride band down relative to the Fermi level along the A-H direction and up along the K- Γ direction, whereas the p -N bands are shifted up. The ARPES spectra calculated within DFT+DMFT successfully reproduce the character of the band dispersion near the Fermi level and agree with an experimental intensity map⁷ better than a simple shift up of the whole band structure obtained using DFT at 0.19 eV as has been proposed in ref 27.

We started the study of the magnetic properties of Ca_2N with the analysis of the behavior of the local spin–spin correlation function $\langle S_z(\tau)S_z(0) \rangle$ on the imaginary-time axis that characterizes the lifetime of the local moment (here $S_z = \sum_{i\sigma\sigma'} \hat{c}_{i\sigma}^\dagger \sigma_{\sigma\sigma'} \hat{c}_{i\sigma'}$, $\hat{c}_{i\sigma}^\dagger$ and $\hat{c}_{i\sigma}$ are the electron creation and destruction operators at orbital i , and spin projection $\sigma, \sigma_{\sigma\sigma'}$ are the Pauli matrices).^{40–42} If the magnetic moments are localized, this correlator which is an average of the product of expectation values of local magnetic moments at different times is constant: $\langle S_z(\tau)S_z(0) \rangle \approx S^2$. Such a behavior was observed for $U = 4 \text{ eV}$ (Figure 5): this function is almost constant, which is typical for strongly correlated compounds with highly localized electronic states. On the other hand, the imaginary time dependence of this correlation function at small values of U indicates the delocalization of spin moments, which is the Fermi liquid regime. In the case of itinerant magnetism or strong fluctuations, the lifetime of an electron in a particular

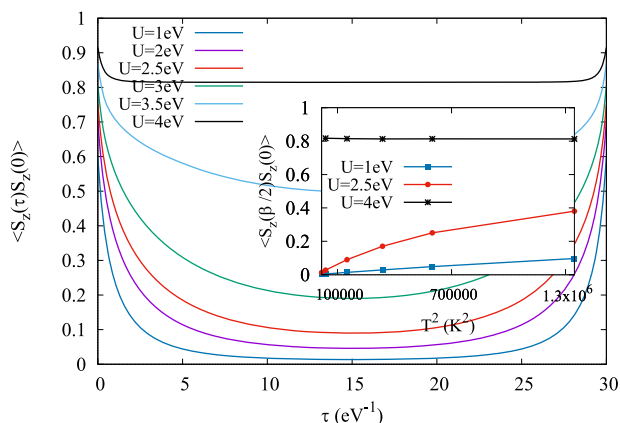


Figure 5. Local spin–spin correlation functions in the imaginary-time domain obtained using DFT+DMFT at $\beta = 30 \text{ eV}^{-1}$ for different values of the Coulomb parameter U . Inset: Dependence of the spin–spin correlation function on T^2 at $\tau = \beta/2$ and $U = 1, 2.5,$ and 4 eV .

state is infinitesimal or the magnitude of the magnetic moment changes rapidly from maximal value to 0 for sufficiently large time intervals. The correlator observed for $U = 1 \text{ eV}$ drops rapidly, which speaks in favor of the weak Coulomb correlations.⁴³ On the other hand, the square of the magnitude of fluctuating moment decreases with decreasing of U values: for $\beta = 30 \text{ eV}^{-1}$ $\langle m_z \rangle^2 = 0.91 \mu_B^2, 0.75 \mu_B^2,$ and $0.60 \mu_B^2$ for $U = 4, 2.5,$ and 1.0 eV , correspondingly. One can see that the magnitude of the magnetic moment does not drop to zero even for $U = 1 \text{ eV}$ which could be explained as a transition from local magnetism toward band magnetism, that is, the electron delocalization and appearance of Stoner instability. The curve of $\langle S_z(\tau)S_z(0) \rangle$ for $U = 2.5 \text{ eV}$, having the closest agreement with the experimental mass enhancement, corresponds to an intermediate correlation strength. The temperature dependence of this correlator can be then used as the measure of the localization, for example in the Fermi liquid regime $\langle S_z(\tau)S_z(0) \rangle \sim T^2/\sin(\pi\tau T)^{244}$ for the τ values that are far enough from 0 and β . $\langle S_z(\beta/2)S_z(0) \rangle$ is a linear function of T^2 for $U = 1 \text{ eV}$, which indicates the Fermi liquid regime, that is, the delocalization (Figure 5 inset). By contrast, for $U = 4 \text{ eV}$ this correlator is temperature-independent, which is expected for a system with localized electrons when the magnitude of the magnetic moments is almost frozen at any temperature. For $U = 2.5 \text{ eV}$, the curve of this correlator lies between those for $U = 1$ and 4 eV , which indicates an intermediate regime with partially localized electrons that is closer to the Fermi liquid at high temperatures.

The local spin susceptibility was calculated as $\chi_{\text{loc}} = g_s^2/3 \cdot \int_0^\beta d\tau \langle \mathbf{S}(0)\mathbf{S}(\tau) \rangle$, where $g_s = 2$ is the electron-spin g -factor and \mathbf{S} is the spin operator. In contrast to the uniform susceptibility, the local spin susceptibility is evaluated within the nonspin-polarized calculations. The behavior of this quantity for different U values repeats the temperature dependence of $\langle S_z(\beta/2)S_z(0) \rangle$, which strengthens the inference that partially localized and relatively large magnetic moments are present in the interstitial sites for $U = 2.5 \text{ eV}$ (Figure 6 inset).

The correlation function $\langle S_z(\tau)S_z(0) \rangle$ calculated at $U = 2.5 \text{ eV}$ for different values of β (Figure 6) shows a similar increase in the localization degree with the increasing temperature: for $\beta = 90 \text{ eV}^{-1}$ (129 K) its curve reminds the one at $U = 1 \text{ eV}$,

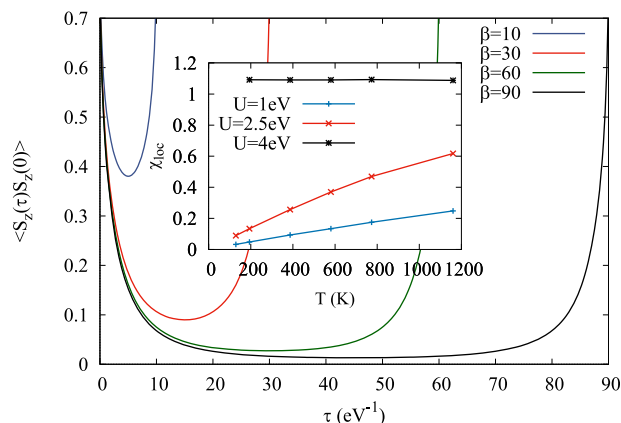


Figure 6. Local spin–spin correlation functions in the imaginary-time domain obtained using DFT+DMFT at $U = 2.5 \text{ eV}$ for different values of β . (Inset) Temperature dependence of the local spin susceptibility at $U = 1, 2.5,$ and 4 eV .

whereas for $\beta = 10 \text{ eV}^{-1}$ (1160 K) its behavior is close to the case at $U = 4 \text{ eV}$. This result is surprising because it contradicts the expectations that temperature should work against the localization. The explanation of this behavior may be found in the specific band structure of the electrider state. A comparison of the DOSes obtained using DMFT for different values of U (Figure 3) shows that the Coulomb correlation leads to a narrowing of the broad DFT band, which should increase the Stoner instability and make a ferromagnetic solution with the band magnetism more preferable. An increase in the temperature acts oppositely, smoothing a sharp quasiparticle peak at the Fermi level, which results in a Stoner instability decrease and a higher localization of the electrider state.

This ambivalent character can be traced in the temperature dependence of the uniform magnetic susceptibility $\chi(T) = m(T)/H_z$, where $m(T) = \sum_i (n_i^\uparrow - n_i^\downarrow)$ is the magnetization (Figure 7) and $n_i^{\uparrow(\downarrow)}$ are the occupancies of i -orbital with spin-

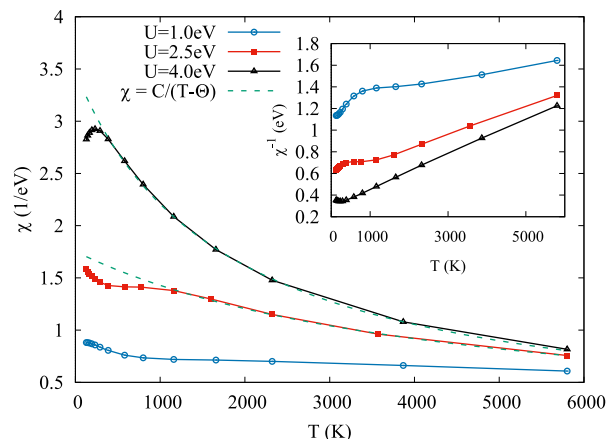


Figure 7. Temperature dependencies of the uniform magnetic susceptibility and its inverse (in the inset).

up (spin-down), calculated using DMFT for $U = 1, 2.5,$ and 4 eV by applying a small external magnetic field to the Hamiltonian and measuring the magnetization.⁴³ The uniform susceptibility strictly follows the Curie–Weiss law for $U = 4 \text{ eV}$, with an estimated Curie–Weiss temperature $\Theta \sim -1700 \text{ K}$, which indicates a substantial antiferromagnetic (AFM) exchange interaction and localized magnetic moments. The

dependence obtained for $U = 2.5$ eV has the same behavior in the high-temperature region, but it exhibits a rapid drop below 500 K and a plateau up to 1200 K. The localization degree at $U = 2.5$ eV is low (Figure 5); we do not imply the presence of any long-range magnetic order, only the AFM fluctuations. The uniform magnetic susceptibility obtained for $U = 1$ eV has a similar drop at low temperatures but is almost constant in the high-temperature region. The shape of the curves may indicate the existence of the band magnetism with a Stoner-type instability recently predicted for several low-dimensional electrifieds⁴⁵ where the magnetic moment and spin density are mainly derived from the interstitial anionic electrons. However, this result means that the magnetism of the electrified states in Ca_2N cannot be described as a conventional band magnetism using the Stoner theory or explained by localized electrons, and a theory combining these two approaches is needed. A similar model has been proposed earlier to describe the magnetism in FeS under pressure.⁴⁶

CONCLUSION

We demonstrated that Coulomb interactions between the electrons confined in two-dimensional cavities are an essential part of the physics that defines the spectral and magnetic properties of layered electrified Ca_2N . The electronic correlations of the layered anionic electrons lead to an increase in the effective electron mass ($2.35m_e$) and to a renormalization and shift of the energy bands near the Fermi level, which agrees with the experimental observations.^{7,27} The local spin susceptibility calculations indicate the existence of nonzero local moments in the electrified states. Due to the correlations, the temperature dependence of the uniform magnetic susceptibility revealed a complex behavior of the magnetic subsystem in which the Stoner-type ferromagnetic instability prevails at low temperatures, and an increase in temperature leads to growing localization of the moments and a strengthening of the antiferromagnetic interaction. We suggest that the observed specific traits of Ca_2N electronic structure and magnetism are expected to be inherent in other two-dimensional electrifieds.

AUTHOR INFORMATION

Corresponding Author

Dmitry Y. Novoselov – M.N. Mikheev Institute of Metal Physics of Ural Branch of Russian Academy of Sciences, Yekaterinburg 620137, Russia; Department of Theoretical Physics and Applied Mathematics, Ural Federal University, Yekaterinburg 620002, Russia; Skolkovo Institute of Science and Technology, Moscow 143026, Russia; orcid.org/0000-0003-1668-3734; Email: novoselov@imp.uran.ru

Authors

Dmitry M. Korotin – M.N. Mikheev Institute of Metal Physics of Ural Branch of Russian Academy of Sciences, Yekaterinburg 620137, Russia; Skolkovo Institute of Science and Technology, Moscow 143026, Russia; orcid.org/0000-0002-4070-2045

Alexey O. Shorikov – M.N. Mikheev Institute of Metal Physics of Ural Branch of Russian Academy of Sciences, Yekaterinburg 620137, Russia; Department of Theoretical Physics and Applied Mathematics, Ural Federal University, Yekaterinburg 620002, Russia; Skolkovo Institute of Science and Technology, Moscow 143026, Russia; orcid.org/0000-0001-7607-6130

Vladimir I. Anisimov – M.N. Mikheev Institute of Metal Physics of Ural Branch of Russian Academy of Sciences, Yekaterinburg 620137, Russia; Department of Theoretical Physics and Applied Mathematics, Ural Federal University, Yekaterinburg 620002, Russia; Skolkovo Institute of Science and Technology, Moscow 143026, Russia

Artem R. Oganov – Skolkovo Institute of Science and Technology, Moscow 143026, Russia; orcid.org/0000-0001-7082-9728

Complete contact information is available at:
<https://pubs.acs.org/10.1021/acs.jpcc.1c04485>

Notes

The authors declare no competing financial interest.

ACKNOWLEDGMENTS

The DFT and MLWF parts of the study were supported by the Ministry of Science and Higher Education of the Russian Federation (No. AAAA-A18-118020190098-5, topic “Electron”). The DMFT calculations were carried out within the state assignment of the Russian Science Foundation (Project 19-72-30043).

REFERENCES

- (1) Dye, J. L.; DeBacker, M. G. Physical and Chemical Properties of Alkalides and Electrifieds. *Annu. Rev. Phys. Chem.* **1987**, *38*, 271–299.
- (2) Toda, Y.; Kim, S. W.; Hayashi, K.; Hirano, M.; Kamiya, T.; Hosono, H.; Haraguchi, T.; Yasuda, H. Intense thermal field electron emission from room-temperature stable electrified. *Appl. Phys. Lett.* **2005**, *87*, 1–3.
- (3) Kitano, M.; Inoue, Y.; Yamazaki, Y.; Hayashi, F.; Kanbara, S.; Matsuishi, S.; Yokoyama, T.; Kim, S.-W.; Hara, M.; Hosono, H. Ammonia synthesis using a stable electrified as an electron donor and reversible hydrogen store. *Nat. Chem.* **2012**, *4*, 934–940.
- (4) Toda, Y.; Hirayama, H.; Kuganathan, N.; Torrisi, A.; Sushko, P. V.; Hosono, H. Activation and splitting of carbon dioxide on the surface of an inorganic electrified material. *Nat. Commun.* **2013**, *4*, 1–8.
- (5) Kitano, M.; Kanbara, S.; Inoue, Y.; Kuganathan, N.; Sushko, P. V.; Yokoyama, T.; Hara, M.; Hosono, H. Electrified support boosts nitrogen dissociation over ruthenium catalyst and shifts the bottleneck in ammonia synthesis. *Nat. Commun.* **2015**, *6*, 1–9.
- (6) Hara, M.; Kitano, M.; Hosono, H. Ru-Loaded C12A7:e⁻ Electrified as a Catalyst for Ammonia Synthesis. *ACS Catal.* **2017**, *7*, 2313–2324.
- (7) Lee, K.; Kim, S. W.; Toda, Y.; Matsuishi, S.; Hosono, H. Dicalcium nitride as a two-dimensional electrified with an anionic electron layer. *Nature* **2013**, *494*, 336–340.
- (8) Guan, S.; Yang, S. A.; Zhu, L.; Hu, J.; Yao, Y. Electronic, Dielectric and Plasmonic Properties of Two-Dimensional Electrified Materials X_2N (X = Ca, Sr): A First-Principles Study. *Sci. Rep.* **2015**, *5*, 12285.
- (9) Yi, S.; Choi, J.-h.; Lee, K.; Kim, S. W.; Park, C. H.; Cho, J.-h. Stacking-sequence-independent band structure and shear exfoliation of two-dimensional electrified materials. *Phys. Rev. B: Condens. Matter Mater. Phys.* **2016**, *94*, 235428.
- (10) Inoshita, T.; Takemoto, S.; Tada, T.; Hosono, H. Surface electron states on the quasi-two-dimensional excess-electron compounds Ca_2N and Y_2C . *Phys. Rev. B: Condens. Matter Mater. Phys.* **2017**, *95*, 165430.
- (11) Inoshita, T.; Tsukada, M.; Saito, S.; Hosono, H. Probing a divergent van Hove singularity of graphene with a Ca_2N support: A layered electrified as a solid-state dopant. *Phys. Rev. B: Condens. Matter Mater. Phys.* **2017**, *96*, 245303.
- (12) Cudazzo, P.; Gatti, M. Collective charge excitations of the two-dimensional electrified Ca_2N . *Phys. Rev. B: Condens. Matter Mater. Phys.* **2017**, *96*, 125131.

- (13) Zeng, X.; Zhao, S.; Li, Z.; Yang, J. Electron-phonon interaction in a Ca_2N monolayer: Intrinsic mobility of electrene. *Phys. Rev. B: Condens. Matter Mater. Phys.* **2018**, *98*, 155443.
- (14) Mortazavi, B.; Berdiyev, G. R.; Shahrokhi, M.; Rabczuk, T. Mechanical, optoelectronic and transport properties of single-layer Ca_2N and Sr_2N electrides. *J. Alloys Compd.* **2018**, *739*, 643–652.
- (15) Kim, Y. J.; Kim, S. M.; Yu, C.; Yoo, Y.; Cho, E. J.; Yang, J. W.; Kim, S. W. Chemoselective Hydrodehalogenation of Organic Halides Utilizing Two-Dimensional Anionic Electrons of Inorganic Electride $[\text{Ca}_2\text{N}]^+ \cdot e^-$. *Langmuir* **2017**, *33*, 954–958.
- (16) Qiu, X. L.; Zhang, J. F.; Lu, Z. Y.; Liu, K. Manipulating the Electronic and Magnetic Properties of Monolayer Electride Ca_2N by Hydrogenation. *J. Phys. Chem. C* **2019**, *123*, 24698–24704.
- (17) Zhang, X.; Yang, G. Recent Advances and Applications of Inorganic Electrides. *J. Phys. Chem. Lett.* **2020**, *11*, 3841–3852.
- (18) Hosono, H.; Kitano, M. Advances in Materials and Applications of Inorganic Electrides. *Chem. Rev.* **2021**, *121*, 3121–3185.
- (19) Novoselov, D. Y.; Anisimov, V. I.; Oganov, A. R. Strong electronic correlations in interstitial magnetic centers of zero-dimensional electride $\beta\text{-Yb}_3\text{Sb}_3$. *Phys. Rev. B: Condens. Matter Mater. Phys.* **2021**, *103*, 235126.
- (20) Hiraishi, M.; Kojima, K. M.; Okabe, H.; Koda, A.; Kadono, R.; Wu, J.; Lu, Y.; Hosono, H. Anomalous diamagnetism of electride electrons in transition metal silicides. *Phys. Rev. B: Condens. Matter Mater. Phys.* **2021**, *103*, L241101.
- (21) Zhou, J.; Shen, L.; Yang, M.; Cheng, H.; Kong, W.; Feng, Y. P. Discovery of Hidden Classes of Layered Electrides by Extensive High-Throughput Material Screening. *Chem. Mater.* **2019**, *31*, 1860–1868.
- (22) Inoshita, T.; Jeong, S.; Hamada, N.; Hosono, H. Exploration for Two-Dimensional Electrides via Database Screening and Ab Initio Calculation. *Phys. Rev. X* **2014**, *4*, 031023.
- (23) Burton, L. A.; Ricci, F.; Chen, W.; Rignanesi, G. M.; Hautier, G. High-Throughput Identification of Electrides from All Known Inorganic Materials. *Chem. Mater.* **2018**, *30*, 7521–7526.
- (24) Tang, H.; Wan, B.; Gao, B.; Muraba, Y.; Qin, Q.; Yan, B.; Chen, P.; Hu, Q.; Zhang, D.; Wu, L.; et al. Metal-to-Semiconductor Transition and Electronic Dimensionality Reduction of Ca_2N Electride under Pressure. *Advanced Science* **2018**, *5*, 2–7.
- (25) Novoselov, D. Y.; Korotin, D. M.; Shorikov, A. O.; Oganov, A. R.; Anisimov, V. I. Interplay Between Coulomb Interaction and Hybridization in Ca and Anomalous Pressure Dependence of Resistivity. *JETP Lett.* **2019**, *109*, 387–391.
- (26) Novoselov, D. Y.; Korotin, D. M.; Shorikov, A. O.; Oganov, A. R.; Anisimov, V. I. Weak Coulomb correlations stabilize the electride high-pressure phase of elemental calcium. *J. Phys.: Condens. Matter* **2020**, *32*, 445501.
- (27) Oh, J. S.; Kang, C. J.; Kim, Y. J.; Sinn, S.; Han, M.; Chang, Y. J.; Park, B. G.; Kim, S. W.; Min, B. I.; Kim, H. D.; et al. Evidence for Anionic Excess Electrons in a Quasi-Two-Dimensional Ca_2N Electride by Angle-Resolved Photoemission Spectroscopy. *J. Am. Chem. Soc.* **2016**, *138*, 2496–2499.
- (28) Kresse, G.; Furthmüller, J. Efficient iterative schemes for ab initio total-energy calculations using a plane-wave basis set. *Phys. Rev. B: Condens. Matter Mater. Phys.* **1996**, *54*, 11169–11186.
- (29) Giannozzi, P.; Baroni, S.; Bonini, N.; Calandra, M.; Car, R.; Cavazzoni, C.; Ceresoli, D.; Chiarotti, G. L.; Cococcioni, M.; Dabo, I.; et al. QUANTUM ESPRESSO: a modular and open-source software project for quantum simulations of materials. *J. Phys.: Condens. Matter* **2009**, *21*, 395502.
- (30) Perdew, J. P.; Burke, K.; Ernzerhof, M. Generalized Gradient Approximation Made Simple. *Phys. Rev. Lett.* **1996**, *77*, 3865–3868.
- (31) Mostofi, A. A.; Yates, J. R.; Pizzi, G.; Lee, Y.-S.; Souza, I.; Vanderbilt, D.; Marzari, N. An updated version of wannier90: A tool for obtaining maximally-localised Wannier functions. *Comput. Phys. Commun.* **2014**, *185*, 2309–2310.
- (32) Cococcioni, M.; de Gironcoli, S. Linear response approach to the calculation of the effective interaction parameters in the LDA+U method. *Phys. Rev. B: Condens. Matter Mater. Phys.* **2005**, *71*, 035105.
- (33) Anisimov, V. I.; Poteryaev, A. I.; Korotin, M. A.; Anokhin, A. O.; Kotliar, G. First-principles calculations of the electronic structure and spectra of strongly correlated systems: dynamical mean-field theory. *J. Phys.: Condens. Matter* **1997**, *9*, 7359–7367.
- (34) Held, K.; Nekrasov, I. A.; Keller, G.; Eyert, V.; Blüner, N.; McMahan, A. K.; Scalettar, R. T.; Pruschke, T.; Anisimov, V. I.; Vollhardt, D. Realistic investigations of correlated electron systems with LDA+DMFT. *Phys. Status Solidi B* **2006**, *243*, 2599–2631.
- (35) Lichtenstein, A. I.; Katsnelson, M. I. Ab initio calculations of quasiparticle band structure in correlated systems: LDA++ approach. *Phys. Rev. B: Condens. Matter Mater. Phys.* **1998**, *57*, 6884–6895.
- (36) AMULET. Advanced Materials Simulation Ekaterinburg's Toolbox. <http://www.amulet-code.org> (accessed 2021-06-20).
- (37) Werner, P.; Millis, A. J. Hybridization expansion impurity solver: General formulation and application to Kondo lattice and two-orbital models. *Phys. Rev. B: Condens. Matter Mater. Phys.* **2006**, *74*, 155107.
- (38) Vidberg, H. J.; Serene, J. W. Solving the Eliashberg equations by means of N-point Padé approximants. *J. Low Temp. Phys.* **1977**, *29*, 179–192.
- (39) Korotin, D. M.; Novoselov, D.; Anisimov, V. I. Correlation effects and phonon modes softening with doping in $\text{Ba}_{1-x}\text{K}_x\text{BiO}_3$. *J. Phys.: Condens. Matter* **2014**, *26*, 195602.
- (40) Igoshev, P. A.; Efremov, A. V.; Poteryaev, A. I.; Katanin, A. A.; Anisimov, V. I. Magnetic fluctuations and effective magnetic moments in γ -iron due to electronic structure peculiarities. *Phys. Rev. B: Condens. Matter Mater. Phys.* **2013**, *88*, 155120.
- (41) Shorikov, A. O.; Poteryaev, A. I.; Anisimov, V. I.; Streltsov, S. V. Hydrogenation-driven formation of local magnetic moments in LaCoO_3 . *Phys. Rev. B: Condens. Matter Mater. Phys.* **2018**, *98*, 165145.
- (42) Novoselov, D. Y.; Korotin, D. M.; Shorikov, A. O.; Anisimov, V. I. Charge and spin degrees of freedom in strongly correlated systems: Mott states opposite Hundas metals. *J. Phys.: Condens. Matter* **2020**, *32*, 235601.
- (43) Belozero, A. S.; Korotin, M. A.; Anisimov, V. I.; Poteryaev, A. I. Monoclinic M_1 phase of VO_2 : Mott-Hubbard versus band insulator. *Phys. Rev. B: Condens. Matter Mater. Phys.* **2012**, *85*, 045109.
- (44) Werner, P.; Gull, E.; Troyer, M.; Millis, A. J. Spin Freezing Transition and Non-Fermi-Liquid Self-Energy in a Three-Orbital Model. *Phys. Rev. Lett.* **2008**, *101*, 166405.
- (45) Sui, X.; Wang, J.; Duan, W. Prediction of Stoner-Type Magnetism in Low-Dimensional Electrides. *J. Phys. Chem. C* **2019**, *123*, 5003–5009.
- (46) Ushakov, A. V.; Shorikov, A. O.; Anisimov, V. I.; Baranov, N. V.; Streltsov, S. V. Suppression of magnetism under pressure in FeS : A DFT+DMFT study. *Phys. Rev. B: Condens. Matter Mater. Phys.* **2017**, *95*, 205116.